Sādhanā (2022) 47:126
https://doi.org/10.1007/s12046-022-01895-2

Effect of wind load on irregular shape tall buildings having different corner configuration

RAHUL KUMAR MEENA, RITU RAJ* and S ANBUKUMAR

Department of Civil Engineering, Delhi Technological University, New Delhi 110042, India
e-mail: rahulkumar_phd2k18@dtu.ac.in; rituraj@dtu.ac.in; sanbukumar@dce.ac.in

MS received 21 December 2021; revised 10 March 2022; accepted 25 April 2022

Abstract. Tall buildings are mainly designed to resist wind loads because wind-induced vibration is more critical for occupant's comfort level on top of the building. Therefore, evaluation of wind-generated pressure is must for such type of tall buildings. Investigation of response due to wind loads on tall buildings is possible by employing numerical modelling such as computational fluid dynamic tools. Regular plan shape structure can be designed for wind load using various international standards and available literatures. In this research comparison is made between four models in which model-A and B is having the regular shape while model-C and D are of irregular shape. These study is useful for the designer to evaluate the response of structures under strong wind conditions. The grid sensitivity and validation study are performed for rectangular shape tall buildings. Validation of the study shows that numerical simulation results are more or less identical with experimental results. In present research work selected building models have equal cross-sectional area and height. Numerical study performed by employing the k-ε turbulence model and the results are compared with the experimental findings. Out of all the four models, the Y-shape model with round in corners has a minimum base moment and the least coefficient of drag.

Keywords. Tall buildings; Irregular shapes; horizontal pressure distribution; Base shear and base moment; CFD; Corner configuration.

1. Introduction

Numerous tall buildings are already being constructed or developing all around the world. Peoples are migrating to urban areas now-a-days. In order to accommodate such big population in cities, many lands are occupied by the building authorities for the construction of high-rise building projects. Construction of these high-rise structures becomes difficult when available land have many irregularities in terms of size and shape. Therefore, the construction of tall buildings having irregular cross-sectional shapes is the better idea to overcome these irregular land problems. Wind effects on such irregular shape high-rise structures are the major concern for the structural designer due to unavailability of wind data. Instead of designing the irregular shape building, the design of regular shape tall buildings is possible through different international standards [1–7]. The available international standards are discussing the wind effects on regular shape structure and silent in case of irregular shape structure. The wind induced effects can be obtained on such irregular structures by two major available options like one is wind tunnel testing [8, 9] and other is computational fluid dynamics methods [10–12]. In this research evaluation of wind effects is done using numerical simulation technique i.e. ANSYS CFX.

Wind effects on high-rise structures have been investigated by many researchers using wind tunnel test like Nagar *et al* [13] executed an experimental study on "H" shaped high rise buildings. Kwok [14] investigated the wind induced response on the various shape of tall buildings. Blessmann and Riera [15] performed the test in wind tunnel and obtained the wind induced response on the interfering tall buildings. Pal *et al* [16] performed the experiment in boundary layer wind tunnel on square plane shape model and remodel triangle shape model of high rise structure. Sharma *et al* [17] presented the techniques of reducing wind load by modifying the corner configuration on tall buildings. Yi and Li [18] studied the wind effects on a super tall building using wind tunnel techniques and compared the result on full scale building. Bairagi and Dalui [19] compared the aerodynamic coefficients of set-back tall building for wind load. Bhattacharyya and Dalui [20] performed experiment and simulation on "E" shape tall building to investigate the mean wind pressure. Bearman and Morel [21] studied the effect of free stream turbulence effect of flow around bluff bodies. Raj and Ahuja [22] performed the experiment on a cross shape tall

*For correspondence
Published online: 28 June 2022

building. Raj *et al* [23] studied the response of square and plus shape building by varying wind load. Li *et al* [24] investigated the wind induced torque on "L" shape tall building. Blackmore [25] explored the design of building structures using wind tunnel method and concluded from experimental research that the design data available in various standards are in adequate. During design of tall building, the evaluation of wind load is necessary for such structures whose design data are absent, building having both the side setback is affected more with respect to single side setback. Limited research work done for interference of the building such as Hui *et al* [26] done the experiment in wind tunnel for two rectangular building model. Pal and Raj [27] evaluated the wind induced interference effect on remodeled shape tall building. Zu and Lam [28] investigated the across wind response of interference for twin tall buildings. Nagar *et al* [29] on two plus plan shape tall building. Gaur *et al* [30] investigated the interference effect on corner configured structure using CFD. Important outcomes from these findings such as pressure distribution for isolated building and as well as in full blockage condition. The interference effect is more on the principal building if the interfering building is located on the upstream of wind. Corner cut model configuration helps to reduce the drag force and flow separation at the principal model.

Investigation of wind effects on irregular shape can be possible by using various available tools such as experimental and numerical methods. However, experimental methods are time consuming and having some types of limitations. Computational fluid dynamics techniques are employed to evaluate the wind effect on such irregular shape high rise structure in order to overcome such limitations. Rajasekarababu and Vinayagamurthy [31] investigated wind effects on setback building. Taniguchi and Akamine [32] analyzed the wind pressure coefficient on detached houses in a dense residential block. Zheng *et al* [33] predicted the improvement of inflow boundary conditions in the numerical simulation to investigate the wind flow around the tall building. Haque *et al* [34] estimated the flow fields around rectangular cylinder under turbulent flow by large eddy simulation turbulence model. Gaur and Raj [35] numerically investigated the wind loads effects on a square shape building model. Mou *et al* [36] performed a numerical simulation to observe the variation in pressure distribution on various building models. Hu *et al* [37] numerically observed the mean wind speed and turbulence intensity effect on tall building using shear stress transport and k-ω turbulence model. Blocken *et al* [38] provided recommendation for accurate CFD simulation for atmospheric boundary layer flow. Bairagi and Dalui [39] evaluated wind generated effect on stepped tall building. Wind induced effect are investigated by various researcher like Kumar and Raj [40] on octagonal plan oval shape building, Okajima [41] on rectangular cylinder, Mallick *et al* [42] on "C" shape, Stathopoulos and Baskaran [43] discussed wind environmental conditions around tall buildings, Cheng *et al* [44] evaluated the wind pressure effect and aerodynamics forces on tall building of square shape, Bhattacharjee *et al* [45] on butterfly plan shape tall buildings, Tang *et al* [46] numerically simulated on polygonal buildings, Zheng and Zhang [47] investigated the drag effects on the controlled suction on high rise building, Bairagi and Dalui [48] on setback building, Raj [49] analyzed the response of plus shaped tall building with different bracing system under wind load, the notable outcomes from these numerical studies are as mean pressure on wind ward face will have positive values while other faces will be under the impact of negative pressure. The height and distance of neighboring buildings contribute significantly to external wind flow patterns. Wake length is the governing factor that controls the drag force on high-rise structures. Numerical computations time can be reduced by employing shear stress transport and k-ω turbulence model and Reynold's number is strongly dependent on the breadth to width ratio of the building model. Pressure distribution patterns are mainly influenced by wind flow at different angle and available terrain surrounding the tall structures. Wind fluctuation increases with the increment in the opening in the high-rise structure and generated drag force decreases by twisting the building model shape. The influence of wind can be reduced on high-rise building by controlling the suction. Building with double side setback is efficient to maintain the velocity at the pedestrian level.

In this research study, two corners modified rectangular regular building model and two corners modified Y-shape irregular building models are considered having equal cross-sectional area and height. Corners having the modification such as corner cut, chamfer and fillet etc. helps to reduce the wind impact on high rise structure because of that in this research a comparative study on chamfer and fillet corners are selected. The numerical analysis on such shapes of high-rise building is performed using ANSYS CFX. A very few amount research is done on such type of comparison and this comparison will help a structural designer to choose the building shape having equal cross-sectional area.

2. Methodology

The numerical investigation is performed on the regular and irregular shape building model using ANSYS CFX, before the starting of the work validation study was carried out and the results are found similar to the experimental results and various international standards.

2.1 *Numerical simulation*

Numerical simulation is performed as per the guidelines available in ANSYS CFX Solver modeling guide [50].

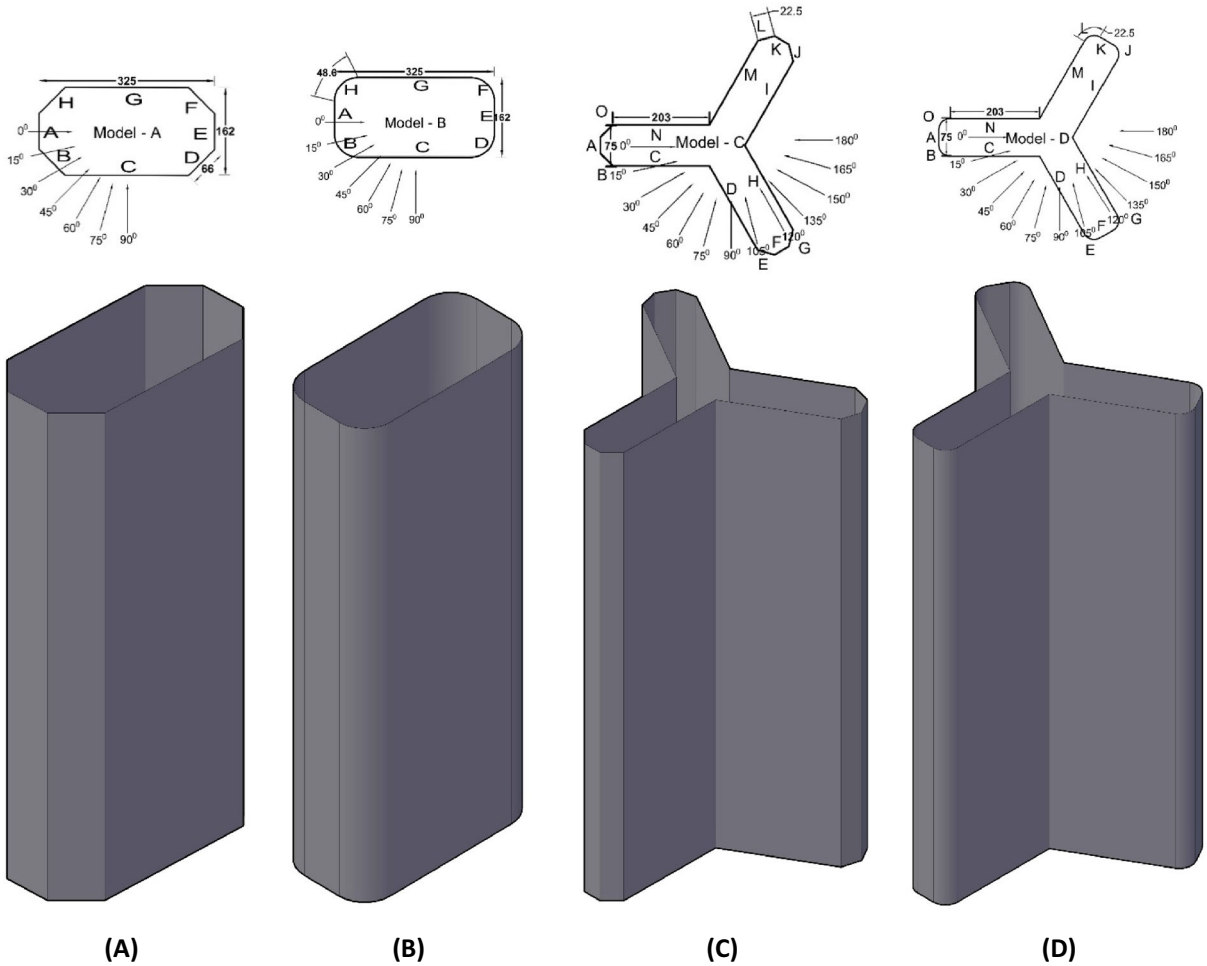

Figure 1. Building model in plan and isometric view.

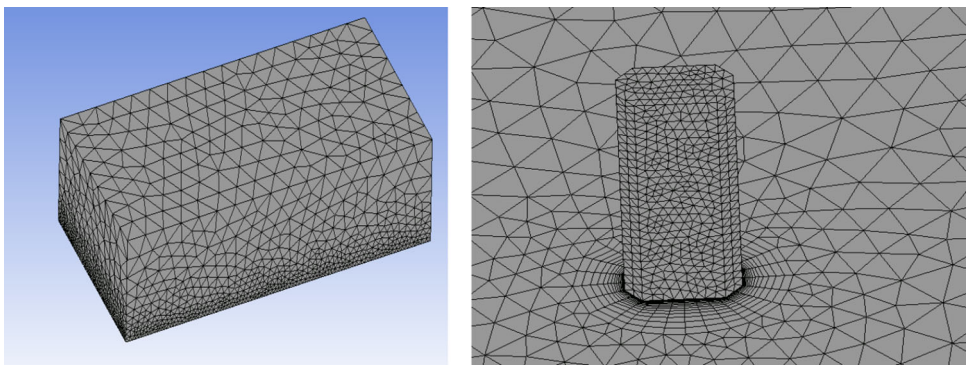

Figure 2. Description of meshing.

Some basic equations are utilized in numerical simulation, such as the Navier Stock equation and continuity equation.Navier Stokes equation

$$\frac{\partial(\rho u_i)}{\partial t} = -\frac{\partial(\rho u_i u_j)}{\partial x_j} - \frac{\partial P}{\partial x_j} + \frac{\partial}{\partial_{x_j}}\left[\mu\left(\frac{\partial_{u_i}}{\partial_{x_j}} + \frac{\partial_{u_j}}{\partial_{x_i}}\right)\right] + F \quad (1)$$

Acceleration term = −Convection term
− Pressure gradient
+ Effects of viscosity + Body force

Continuity equation

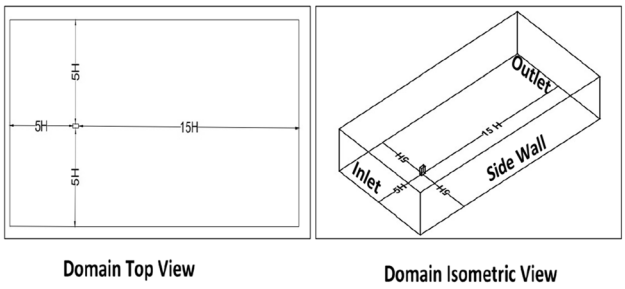

Figure 3. Domain.

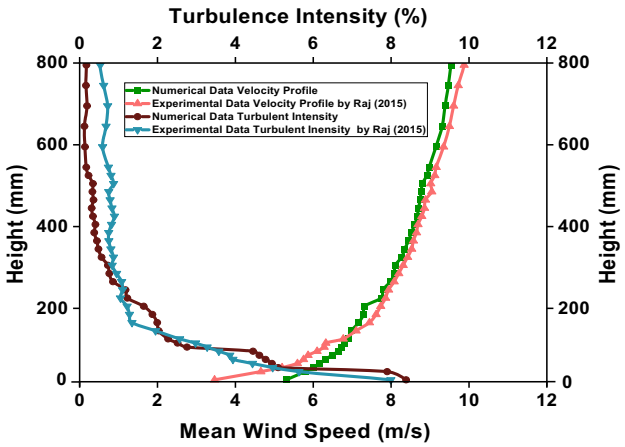

Figure 4. Mean wind speed and turbulent intensity profile numerical simulation and experimental.

$$\frac{\partial_\rho}{\partial_t} + \frac{\partial_{\rho_i}}{\partial_{x_i}} = 0 \tag{2}$$

Eddy viscosity

$$\mu_{t=}\rho c_\mu \frac{k^2}{\in} \tag{3}$$

where c_μ is the dimensionless constant;

This research study is performed by utilizing the k-ε turbulence model, which is two-equation model.

The standard k-ε model uses the following transport equations for the turbulence kinetic energy and turbulence dissipation rate:

$$\frac{\partial(\rho k)}{\partial t} + \frac{\partial}{\partial x_j}(\rho U_j k) = \frac{\partial}{\partial x_j}\left[\left(\mu + \frac{\mu_t}{\sigma_k}\right)\frac{\partial k}{\partial x_j}\right] + P_k - \rho\varepsilon + P_{kb} \tag{4}$$

$$\frac{\partial(\rho\varepsilon)}{\partial t} + \frac{\partial}{\partial x_j}(\rho U_j \varepsilon) = \frac{\partial}{\partial x_j}\left[\left(\mu + \frac{\mu_t}{\sigma_k}\right)\frac{\partial \varepsilon}{\partial x_j}\right] + \frac{\varepsilon}{k}(C_{\varepsilon 1}P_k - C_{\varepsilon 2\rho\varepsilon} + C_{\varepsilon 1}P_{\varepsilon b}) \tag{5}$$

where $C_{\varepsilon 1}, C_{\varepsilon 2}, \sigma_k$ *and* σ_ε are constant; P_{kb} and $P_{\varepsilon b}$ Represent the influence of the buoyancy forces; P_k Turbulence production due to viscous forces, which is modeled using.

$$P_k = \mu\left(\frac{\partial U_i}{\partial x_j} + \frac{\partial U_j}{\partial x_i}\right)\frac{\partial U_i}{\partial x_j} - \frac{2}{3}\frac{\partial U_k}{\partial x_k}\left(3\mu_t\frac{\partial U_k}{\partial x_k} + \rho k\right) \tag{6}$$

2.2 *Model*

The irregular shape building models are depicted in figure 1 with dimensions and wind incidence angles. The aim of this study is to investigate the wind effects on equal area model by keeping the same ratio of modifications. For these purpose the dimension of such corners and the height of buildings model are same. Models are prepared in ANSYS, CFX design modular by designing the geometry and then extrude of 750 mm height is applied for each case of the tall building model.

2.3 *Meshing*

Meshing plays a very important role in numerical simulation and done as per the available guidelines in ANSYS Meshing User's Guide [51], meshing is of two types, structured that follows a fix pattern of mesh and this is generally hex or quad meshing. Unstructured mesh that does not follow the uniform pattern and sometimes it may produce the irrelevance results. Poor meshing will give error in numerical simulation or will require more computational resources also there may be a chance of bad solution thus for this study the meshing adopted in this numerical simulation is demonstrated in figure 2. The

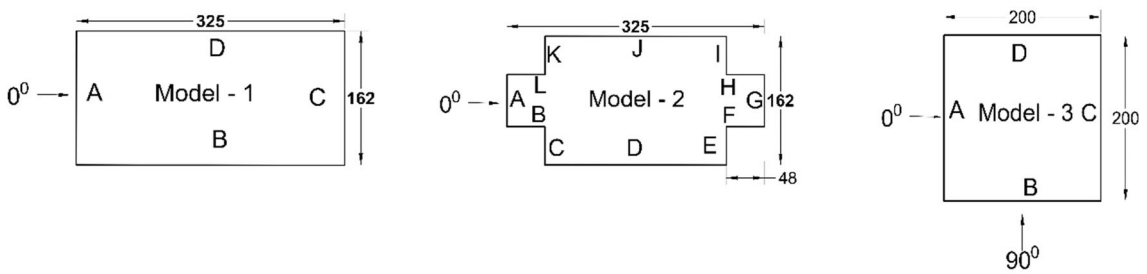

Figure 5. Validation model with dinemsions.

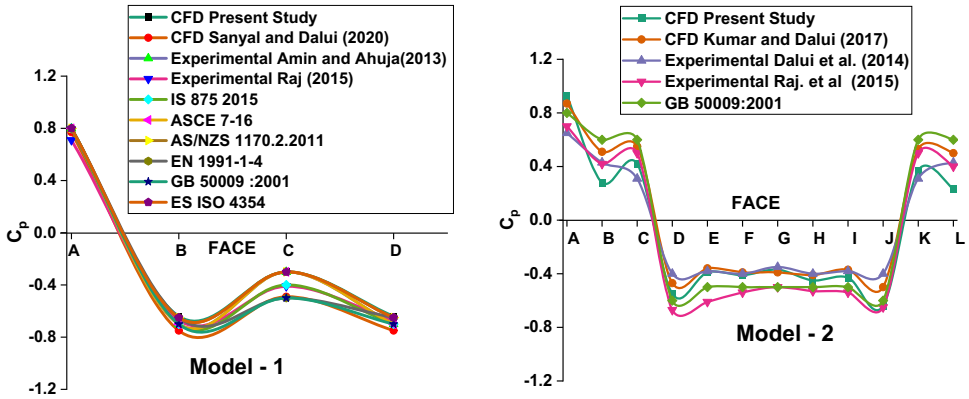

Figure 6. Results validation with experimental and different international standards.

Table 1. Comparison of face average pressure coefficient (C_p) on the model-3 of tall building.

International code	Wind angle	Windward side	Side wall	Leeward side
CFD Results	0°	0.78	−0.64	−0.30
	90°	0.7	−0.61	−0.45
Experimental Result (Raj. 2015, Pal *et al*, and Nagar *et al*)	0°	0.71	−0.67	−0.41
	90°	0.73	−0.66	−0.42
IS 875 (Part 3)	0°	0.7	−0.7	−0.4
	90°	0.8	−0.5	−0.1
ASCE/SEI 7-16	0°	0.8	−0.7	−0.5
	90°	0.8	−0.7	−0.5
AS/NZS 1170.2.2011	0°	0.8	−0.65	−0.5
	90°	0.8	−0.65	−0.5
EN 1991-1-4	0°	0.8	−0.5	−0.7
	90°	0.8	−0.5	−0.7
BS 6399-2	0°	0.8	−0.5	−0.7
	90°	0.8	−0.5	−0.7
GB 50009-2001	0°	0.8	−0.5	−0.7
	90°	0.8	−0.5	−0.7
NSCP 2015	0°	0.8	−0.5	−0.7
	90°	0.8	−0.5	−0.7
ES/ISO 4354: 2012	0°	0.8	−0.65	−0.7
	90°	0.8	−0.65	−0.7

Table 2. Grid convergence test result for model-1.

			Mean external pressure							
			Face				% Error			
Name	Type of meshing	No of elements	A	B	C	D	A	B	C	D
GC-1	Coarse	957324	0.59	−0.49	−0.24	−0.49	36%	32%	26%	32%
GC-2	Medium-1	1284687	0.73	−0.56	−0.27	−0.56	10%	16%	12%	16%
GC-3	Medium-2	1439589	0.78	−0.64	−0.30	−0.64	3%	2%	0%	2%
GC-4	Medium-3	1561140	0.81	−0.69	−0.32	−0.69	1%	5%	6%	5%
GC-5	Fine	2497236	1.02	−0.98	−0.43	−0.98	33%	33%	30%	33%

meshing on building is finer than the ground meshing and domain meshing while inflation is also provided to capture the flow behaviour more accurately. Very fine meshing will need more time and high-end computational resources to perform the simulation and it's not mandatory that very fine meshing will generate the accurate solution while this may produce the irrelevant results.

2.4 *Domain*

The domain is the environment where the numerical simulation is performed. Various recommendations are available for constructing the domain such as Zidan *et al* [52] optimize the fluid domain in CFD simulation for tall buildings, domain used in this study is presented with dimensions in figure 3, this domain is constructed on the recommendation provided by Revuz *et al* [53] also the most of the studies in the past is already produces the numerical simulation results on the basis of domain presented in figure 3.

The sidewall and inlet of the domain are kept at 5H. The outlet is at 15H and height of the domain is at 6H, where H is the height of the building model, such large domain is constructed in the design modular for proper wake generation behind the building model. The sidewall and top are assigned as free slip. Ground of the domain where building model is placed and the wall of the building models are assigned as no-slip wall, free slip wall means that velocity is same as that of the inlet and no-slip means that the velocity distributed as per the power low defined at the inlet.

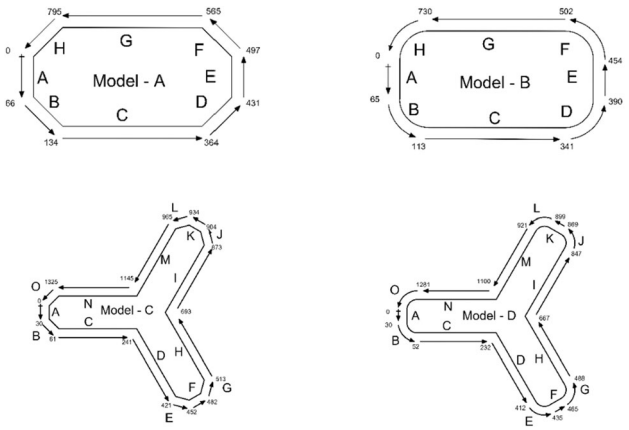

Figure 7. Peripheral distance along the building model-A, model-B, model-C and model-D.

2.5 *Turbulent intensity and mean wind speed profile*

Wind incident on tall buildings is followed by power-law index of wind distribution available for all types of terrain. Generally, wind speed is increases with respect to height and wind speed on the ground is almost zero due the obstruction faces at ground level. Wind velocity become gradient height becomes constant and this is known as free stream wind or gradient wind. Mean wind speed and turbulent intensity are presented in figure 4, the boundary conditions are kept similar with those experimental performed by Raj [54] in boundary layer wind tunnel and comparative graph is also presented to validate the numerical study with the experimental study.

Mean wind speed and turbulent intensity profile should be defined at the inlet to performed the numerical simulation. The boundary layer mean wind speed profile is governed by the power-law equation (eq.7) and the same is applied in the numerical simulation.

$$U = U_h\left(\frac{Z}{Z_H}\right)^{\alpha} \tag{7}$$

where U_h is the boundary layer velocity, which is 10 m/s for this study; Z is the reference height; U is the mean wind speed at a reference height Z; α is a parameter that varies with ground roughness. (Known as power law index); Z_H is the boundary layer depth;

$$I_z = \frac{\sigma_z}{U(z)} \tag{8}$$

where I_z is the turbulence intensity at height z; σ_z is the standard deviation of the wind speed at height z; $U(z)$ is the mean wind speed at height z.

2.6 *Validation*

The solution obtained with the help of numerical techniques are validated with three standards models represented in figure 5. Numerical findings are depicted in the graphical form in figure 6 and table 1. Results presented in paper are identical with experimental and different international standards.

The results of mean C_p are calculated and compared with experimental study performed by Amin and Ahuja [55], Raj [54], Raj *et al* [23] as well as with the numerical finding of Sanyal and Dalui [56], Kumar and Dalui [57] and the result on model-1 is compared with different international standards [1–3, 5, 6, 58].

The external pressure coefficient " C_p" is calculated using the equation (9).

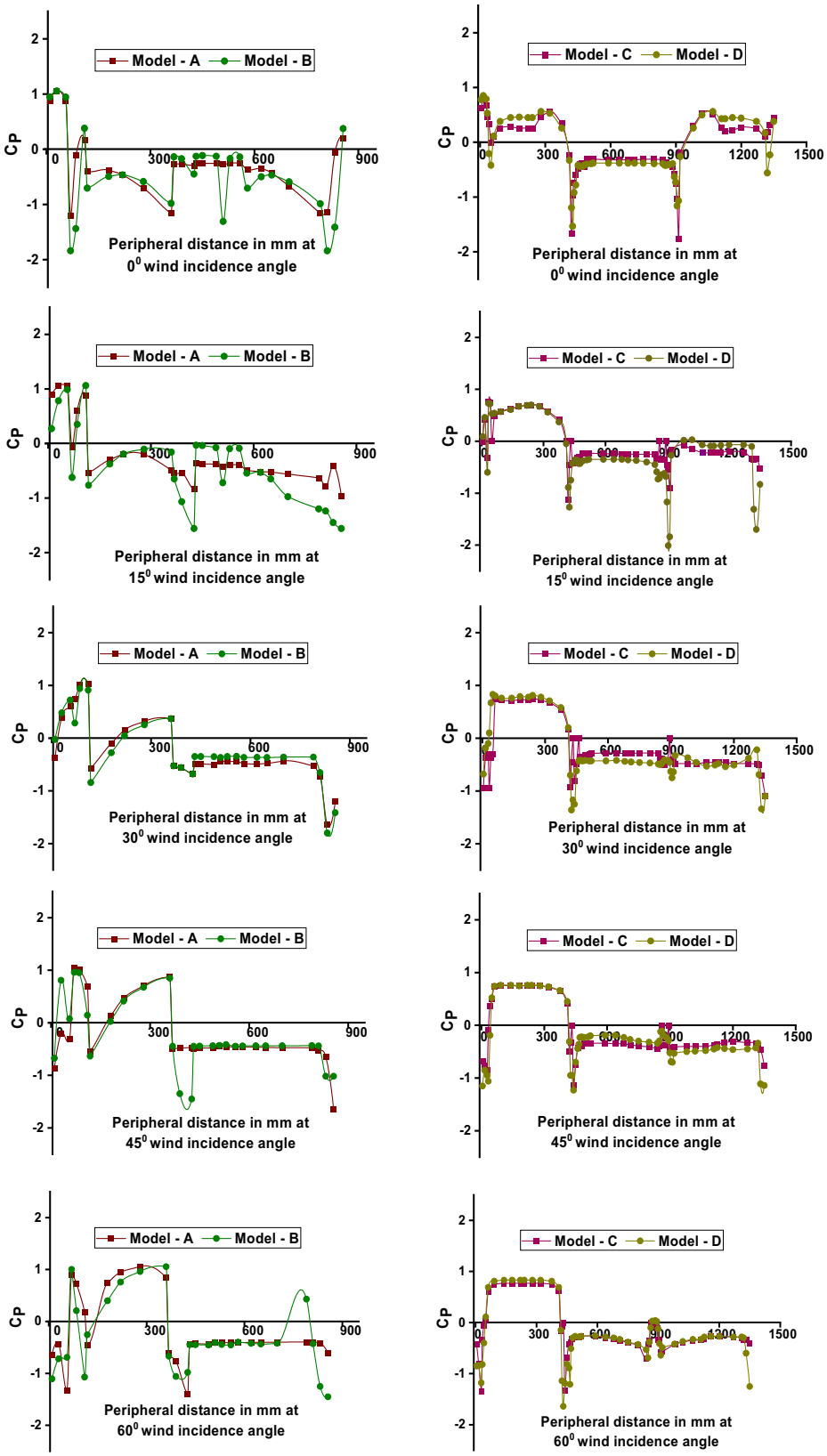

Figure 8. Pressure distribution along with the peripheral distance for model-A, model-B, model-C and model-D.

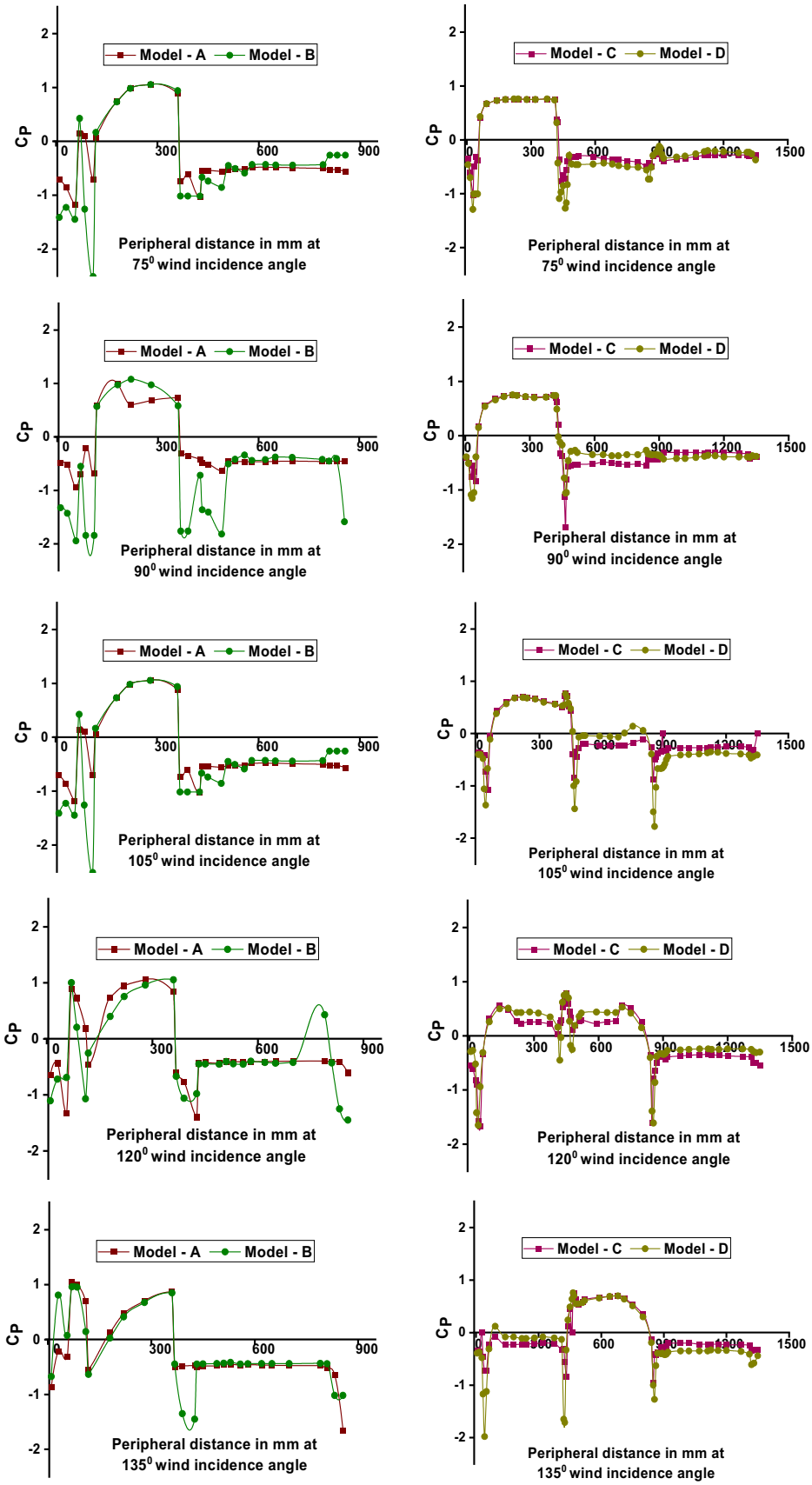

Figure 8. continued

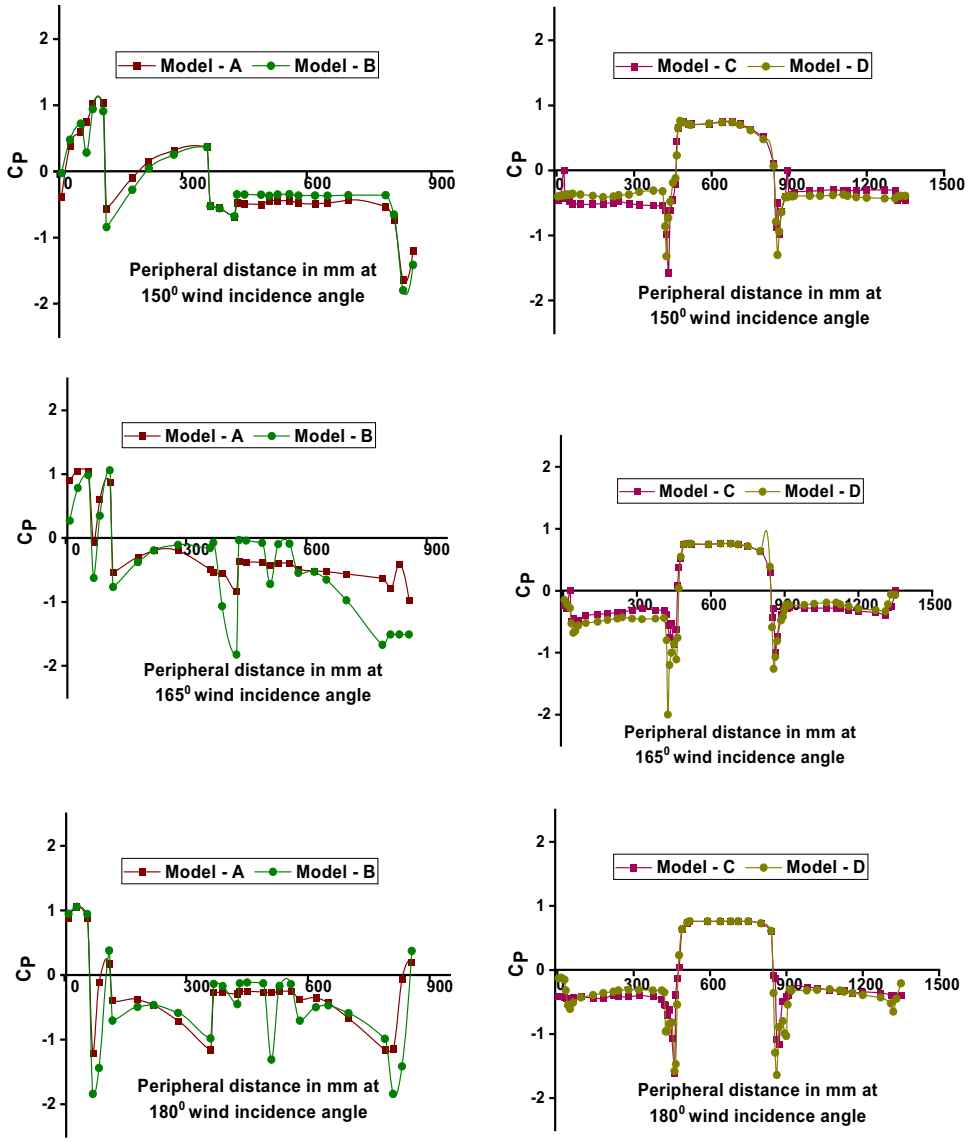

Figure 8. continued

$$C_p = \frac{p - p_o}{\frac{1}{2}\rho U_H{}^2} \tag{9}$$

2.7 *Grid convergence*

In this study a grid convergence study was performed on model-1. Grid convergence study is necessary for a CFD programming as it helps to know the accuracy of CFD solver settings. For the present study GC-3 is adopted for all the wind incidence angle varies from 0° to 180° at the interval of 15° each. In this study the grid convergence study is performed on the basis of procedure provided by Celik *et al* [59], Derakhshandeh and Alam [60]. The percentage error is reported in the table 2 and GC-3 is adopted because of the less percentage error reported in the mean Cp compared with the IS: 875 (part-3): 2015 [5] for 0° wind incidence angle. The grid convergence study is performed on five different cases by varying the meshing type namely coarse, medium and fine. Number of elements for coarse, medium and fine meshing are 957324, 1439589 and 2497236 respectively. Grid convergence study is performed on model-1 while for validation purposes the three model are taken into consideration and validation study is performed on model-1, 2 and 3.

3. Result and discussion

Results of pressure distribution and velocity streamlines are discussed and presented in a graphical and external Cp is tabulated for the building model- A, model- B, model- C and model- D.

3.1 *Horizontal pressure distribution at mid height of building models*

The pressure distribution along the peripheral distance for various building models are presented in figure 7. The pressure distribution along peripheral length are presented at mid height of building in form of graph at 0° to 180° at an interval of 15°. The pressure distribution for building model-A and model-B is of same nature for 90° winds. Figure 8 presented the pressure distribution for model-A, model-B, model-C and model-D. Face-A under the direct exposure to wind depicted positive pressure distribution throughout the face and it is seen that the maximum positive pressure for model-A is 1.05 on face-A at 0° and 15° wind incidences while for face-B at 45° and face-C at 60° & 75° wind incidence angles. The minimum pressure of −1.64 is noted at 832 mm on face-H at 30° wind, which is 156 % less from the maximum positive pressure.

The maximum positive pressure for model-B, is 1.07 at 220 mm which is generated at face-C in case of 90° wind incidence angle and the minimum negative pressure is −1.94 noted on face-A in the case of 90° wind incidence angle at 56 mm of peripheral distance, maximum negative pressure observed on model-B that is almost 180 % of maximum positive pressure. It can be concluded from the results that model-A is more efficient in terms of pressure distribution with respect to model-B having fillet corners. Y- shape building model with chamfer corners i.e. model-C having the maximum pressure of 0.79 at 15 mm and 450 mm peripheral distance on face-A in case of 90° & 120° wind incidence angle respectively.

The minimum pressure of −1.76 which is more than maximum positive pressure on model-C, and similar observation found at 912 mm peripheral distance in case of model-D at 0° wind angle. Y- shape with round corner in each limb having the maximum and minimum pressure of 0.85 at 15 mm and −2.01 detect at 905 mm on face-A at 0° wind angle respectively. Among the model-C and model-D the maximum efficient model is model-C which is having the chamfer shape in each limb of irregular Y- shape.

3.2 *Velocity streamlines*

The Velocity streamlines are presented pictorially for model-A (Rectangular Chamfer) in figure 9 from 0° to 90° wind incidence angle at 15° intervals. Streamlines are obtained from ANSYS CFX Post processing. The wind flow pattern is clearly presenting the size of wake in downstream of the wind, maximum wake is observed for 90° winds as the model is obstructing more wind flow with respect to 0° wind angle and thus the wake is increasing. The pattern of vortex formed in the downstream is changing at each wind angle also, the reattachment of the flow is more in the case of 0° wind.

3.3 *Numerical simulation ISO surface of pressure*

The ISO-surface of pressure is a three-dimensional visualization which present the physical shape of pressure distribution around the building model and is obtained through ANSYS CFX Post by applying Q-Criterion [61, 62]. The ISO-surface of pressure is generated and presented in figure 10 for building model- A, model- B, model- C and model- D.

3.4 *External pressure coefficient*

The external pressure coefficient on the high-rise structure helps designer to calculate the wind effects on such tall buildings. External pressure coefficient for building model-A i.e., rectangular chamfer shown in figure 11 and numerical output are presented in table 3. After the observation face-B and face-H have slightly similar pressure coefficients. The highest pressure observed at 0° wind angle and it is found (0.91) on the face-A, smallest pressure (−1.11) is spot on face-A in case of 75° wind incidence angle. The external pressure coefficient is more or less equivalent with each other in the case of wind ward faces (the face which is in the directly exposure to wind). It is discovered that identical face having uniform pressure coefficient for particular wind incidence angle.

The External pressure coefficient evaluated for building model-B presented in figure 11 (Rectangular fillet) is tabulated in table 4, at 0° to 90° wind incidence angles at the interval of 15°. Maximum positive pressure (0.71) is detected on face-A at 0° wind incidence angle while the least pressure (-1.49) is noticed on face- B and face- D in the case of 90° wind incidence angle.

The external pressure coefficient calculated and tabulated in table 5 for building model-C (Y-shape Chamfer) presented in figure 12. Research study is done on Y- shape for 0° to 180° wind incidence angle while for rectangular model 0° to 90° wind incidence angle. The external pressure coefficient is presented in a tabular form in table 3, the highest pressure (0.69) is observed at face-C in the case of 45° wind incidence and minimum pressure (−1.14) is noticed on face-E, at 150° wind. This is concluded that symmetric face is having identical nature of pressure distribution are observed for 0°, 60°, 120° and 180° wind. for building model-D (Y-shape Fillet) represented in figure 12, the external pressure coefficients are tabulated in table 6,

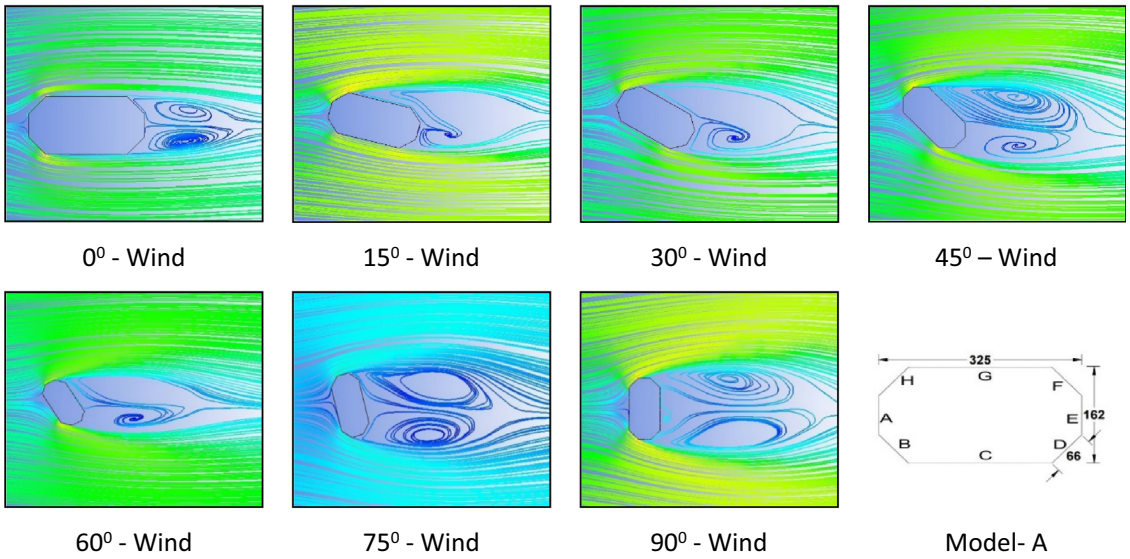

Figure 9. Velocity Streamlines for model-A at 0° to 90° wind incidence angles at an interval of 15°

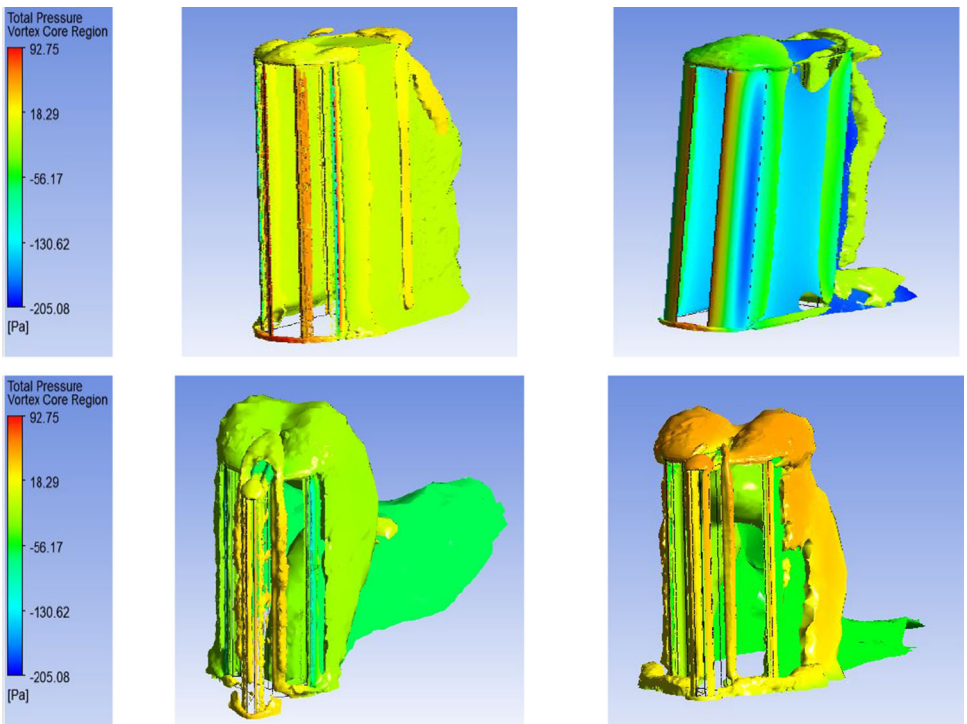

Figure 10. ISO Surface of Pressure around building model-A, model-B, model-C and model-D.

Figure 11. Building models (A) Rectangular Chamfer and (B) Rectangular Fillet.

the maximum pressure (0.69) is noticed on the face-A, face-C, face-D, face-F and face-H at 0°, 45°, 75°, 120° and 165° respectively and minimum pressure (−1.4) on face-L in the case of 15° wind incidence angle. The maximum positive pressure for building models- B and C is nearly of same magnitude on the wind ward face while in the case of negative pressure it is 22 % more for model- D with respect to model- C.

Table 3. External pressure coefficient for building model-A (Rectangular chamfer).

Model-A (Rectangular chamfer)							
Face	0°	15°	30°	45°	60°	75°	90°
A	**0.91**	**0.83**	0.21	−0.36	−0.78	**−1.11**	**−0.50**
B	−0.30	0.46	**0.89**	**0.87**	**0.57**	−0.12	−0.45
C	**−0.59**	−0.32	0.02	0.29	0.19	**0.71**	**0.82**
D	−0.32	−0.46	−0.52	**−0.69**	**−1.12**	−0.76	−0.45
E	−0.28	−0.37	−0.45	−0.46	−0.46	−0.51	**−0.50**
F	−0.32	−0.42	−0.44	−0.45	−0.4	−0.48	−0.41
G	**−0.59**	−0.54	−0.47	−0.43	−0.42	−0.44	−0.42
H	−0.30	**−0.65**	**−0.99**	−0.83	−0.50	−0.45	−0.41

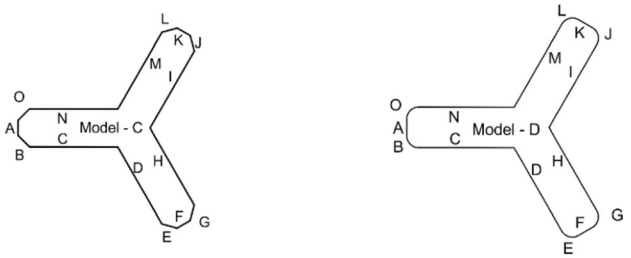

Figure 12. Building models (C) Y-shape Chamfer and (D) Y-shape Fillet.

3.5 *Base shear*

Base shear is derived from the results obtained through the computational fluid dynamic tool ANSYS CFX. The force is calculated on the base and presented in graphical form in figure 13 for the building models considered in this study. The largest base shear along x-direction that is a drag for model- A is 1.84 for at 45° and 135° while for model- B the maximum drag is 1.68 at 30° and 135° in the case of the model- C the drag of 0.65 is maximum at 60° and 180°. The

Table 4. External pressure coefficient for building model-B (Rectangular fillet).

Model-B (Rectangular fillet)							
Face	**0°**	**15°**	**30°**	**45°**	**60°**	**75°**	**90°**
A	**0.71**	**0.51**	0.28	0.05	−0.59	−0.92	−0.99
B	−0.76	0.18	**0.50**	**0.49**	**0.04**	−0.74	**−1.49**
C	−0.45	−0.24	−0.08	0.19	**−1.48**	**0.56**	**0.61**
D	−0.40	−0.78	−0.39	**−1.24**	−0.32	**−1.48**	**−1.49**
E	−0.11	−0.09	−0.29	−0.31	−0.35	−0.41	−0.99
F	−0.40	−0.23	−0.32	−0.32	−0.35	−0.41	−0.60
G	−0.45	−0.59	−0.32	−0.32	−0.32	−0.34	−0.32
H	**−0.76**	**−1.94**	**−1.22**	**−1.24**	−1.06	−0.83	−0.60

Table 5. External pressure coefficient for building model-C (Y-shape Chamfer).

Model-C (Y-shape Chamfer)													
Face	0°	15°	30°	45°	60°	75°	90°	105°	120°	135°	150°	165°	180°
A	**0.65**	−0.06	−0.60	**−0.66**	**−0.87**	−0.62	−0.60	−0.45	−0.45	−0.41	−0.45	−0.32	−0.34
B	0.19	0.47	−0.60	0.26	−0.14	−0.38	−0.69	**−0.77**	**−1.08**	**−0.71**	−0.60	−0.46	−0.39
C	0.20	**0.54**	**0.66**	**0.69**	**0.67**	0.62	0.53	0.43	0.20	−0.12	−0.46	−0.39	−0.35
D	0.23	0.43	0.54	0.62	**0.67**	**0.69**	**0.66**	**0.53**	0.21	−0.25	−0.59	−0.35	−0.30
E	**−1.06**	−0.59	−0.43	−0.26	−0.14	0.14	0.41	0.51	0.25	−0.29	**−1.14**	−0.58	−0.15
F	−0.49	−0.46	−0.53	−0.65	**−0.87**	**−0.63**	−0.65	0.17	**0.66**	0.34	−0.42	**−0.65**	**−0.75**
G	−0.40	−0.36	−0.36	−0.29	−0.32	−0.44	**−0.99**	−0.53	0.25	**0.63**	0.53	0.30	−0.21
H	−0.34	−0.31	−0.31	−0.28	−0.34	−0.35	−0.59	−0.24	0.21	0.54	**0.66**	**0.69**	**0.66**
I	−0.34	−0.32	−0.31	−0.34	−0.45	−0.39	−0.48	−0.11	0.20	0.38	0.50	0.60	**0.66**
J	−0.40	−0.27	−0.33	−0.27	−0.39	−0.40	−0.60	−0.61	**−1.08**	−0.60	−0.74	−0.58	−0.21
K	−0.49	−0.41	−0.45	−0.32	−0.29	−0.31	−0.47	−0.41	−0.45	−0.41	−0.47	−0.45	**−0.75**
L	**−1.06**	**−0.73**	−0.58	−0.43	−0.39	−0.29	−0.45	−0.38	−0.44	−0.36	−0.39	−0.26	−0.15
M	0.23	−0.09	−0.42	−0.39	−0.45	−0.32	−0.35	−0.32	−0.39	−0.30	−0.35	−0.26	−0.30
N	0.20	−0.25	−0.56	−0.35	−0.34	−0.26	−0.35	−0.32	−0.39	−0.31	−0.34	−0.32	−0.35
O	0.19	−0.40	**−0.84**	−0.52	−0.32	−0.26	−0.31	−0.25	−0.44	−0.28	−0.35	−0.25	−0.39

Table 6. External pressure coefficient for building model-D (Y-shape fillet).

Model-D (Y-shape fillet)													
Face	0°	15°	30°	45°	60°	75°	90°	105°	120°	135°	150°	165°	180°
A	**0.69**	0.01	−0.37	**−0.94**	**−0.96**	−0.86	−0.58	−0.41	−0.39	−0.44	−0.39	−0.36	−0.30
B	−0.06	**0.58**	0.39	−0.25	−0.66	**−1.24**	−0.76	−0.95	**−1.28**	**−1.18**	−0.67	−0.51	−0.46
C	0.31	0.54	**0.65**	**0.69**	**0.67**	0.62	0.53	0.41	0.24	−0.06	−0.26	−0.49	−0.42
D	0.26	0.41	0.53	0.62	**0.67**	**0.69**	**0.65**	0.53	0.32	−0.11	−0.43	−0.48	−0.36
E	**−0.89**	−0.90	−0.87	−0.74	−0.66	−0.39	0.33	**0.60**	0.02	−1.07	**−0.98**	−1.20	−0.77
F	−0.39	−0.39	−0.57	−0.84	**−0.96**	−0.99	−0.42	0.34	**0.69**	0.42	−0.31	−0.94	**−0.96**
G	−0.36	−0.33	−0.32	−0.38	−0.79	−0.79	**−0.94**	**−1.01**	0.02	**0.59**	0.47	−0.07	−0.78
H	−0.29	−0.3	−0.32	−0.3	−0.36	−0.47	−0.4	−0.06	0.32	0.54	**0.65**	**0.69**	**0.68**
I	−0.29	−0.32	−0.35	−0.37	−0.43	−0.49	−0.25	−0.01	0.24	0.37	0.50	0.60	**0.68**
J	−0.36	−0.48	−0.33	−0.34	−0.44	−0.52	−0.63	**−1.01**	**−1.28**	−0.92	−0.9	**−0.94**	−0.78
K	−0.39	−0.49	−0.35	−0.36	−0.25	−0.36	−0.34	−0.38	−0.39	−0.36	−0.4	−0.66	**−0.96**
L	**−0.89**	−1.40	−0.87	−0.51	−0.44	−0.34	−0.33	−0.35	−0.35	−0.35	−0.31	−0.37	−0.77
M	0.26	−0.03	−0.23	−0.48	−0.43	−0.37	−0.35	−0.31	−0.30	−0.31	−0.31	−0.3	−0.36
N	0.31	−0.10	−0.40	−0.47	−0.36	−0.30	−0.32	−0.31	−0.30	−0.33	−0.34	−0.37	−0.42
O	−0.06	**−1.23**	**−1.02**	−0.87	−0.79	−0.40	−0.32	−0.35	−0.35	−0.55	−0.34	−0.32	−0.46

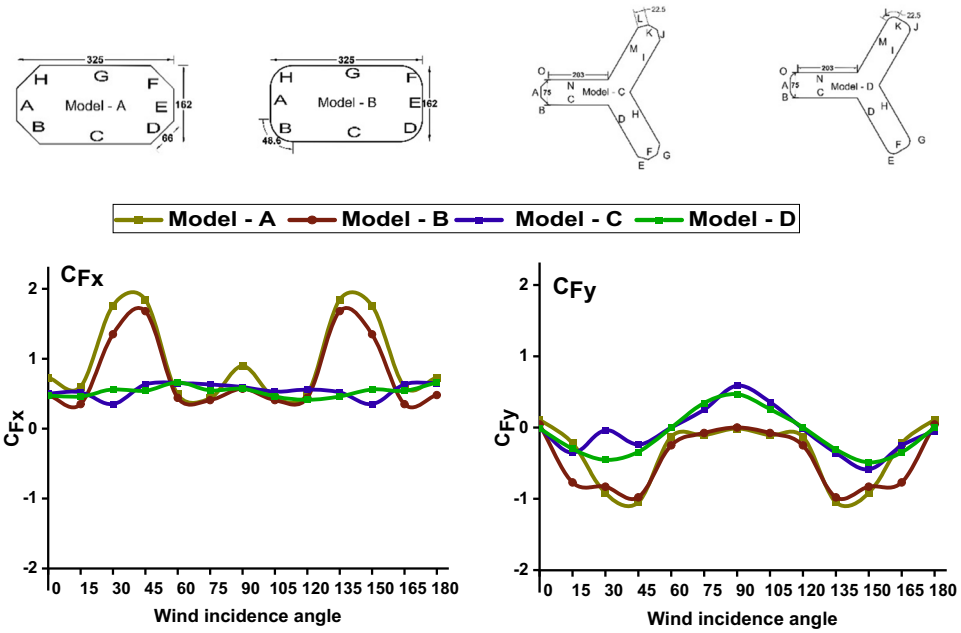

Figure 13. Drag and Lift Force coefficient for model-A, model-B, model-C and model-D at 0° to 180° wind incidence angle.

drag of 0.66 is found maximum for model-D at 60° and 180° wind incidence angles. Lift force is calculated and presented in figure 13 the minimum lift force is found −1.05 for model-A at 45° and 135° while on model-B the least lift force is −0.98 at 45° and 135° wind incidence angles.

Y-shape model-C having chamfer edges at the end of each limb is having the highest and lowest lift as 0.58 at 90° and −0.25 at 165° respectively, while the model- D having round in corner in each limb of Y-shape having the maximum lift of 0.46 and it is spotted at 90° and minimum of −0.45 in noted at 30° winds. Base shear in x and y direction are C_{f_x} & C_{f_y} and it is calculated using equation 10 and equation 11 where F_x & F_y is the base force obtained through numerical simulation, U_h is the reference wind speed at height h and A_p is the projected area.

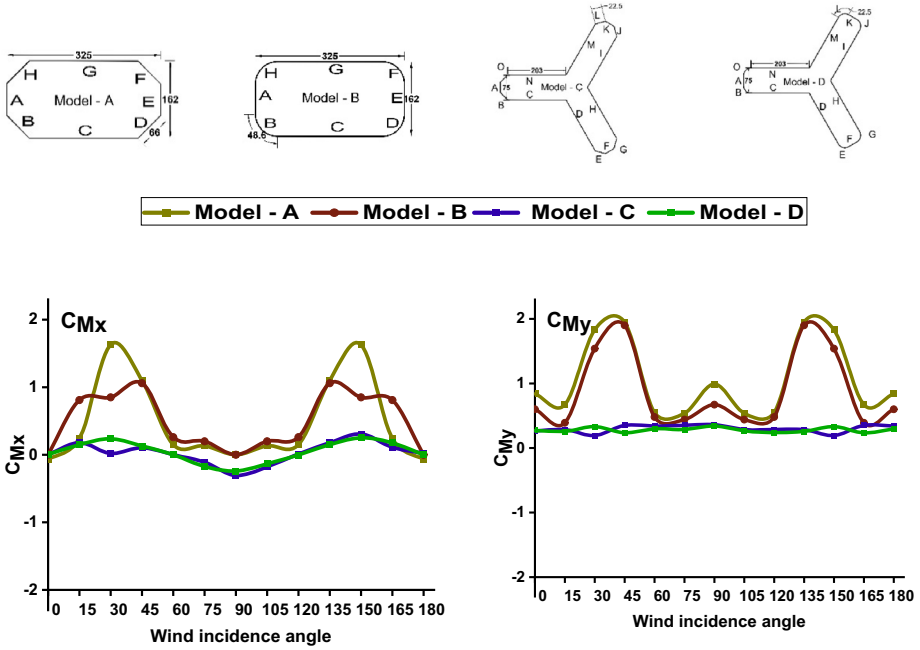

Figure 14. Base moment along X (C_{Mx}) and Y (C_{My}) for model-A, model-B, model-C and model-D at 0° to 180° at an interval of 15° wind incidence angle.

$$C_{f_x} = \frac{F_x}{(0.5\rho_{U_h{}^2}.A_p)} \tag{10}$$

$$C_{f_y} = \frac{F_y}{(0.5\rho_{U_h{}^2}.A_p)} \tag{11}$$

$$C_{M_x} = \frac{M_x}{(0.5\rho_{U_h{}^2}.A_p.H)} \tag{12}$$

$$C_{M_y} = \frac{M_y}{(0.5\rho_{U_h{}^2}.A_p.H)} \tag{13}$$

3.6 *Base moment*

The base moment for model-A, B, C & D are presented in figure 14, moments are calculated at the base of the building model. The maximum M_x is 1.63 for model-A at 30° and 150° wind while for model-B is 1.06 at 45° and 135° wind incidence angle. The greatest C_{Mx} for model- C is 0.30 at 90° and 150° wind while for model-D the maximum is 0.25 at 150° wind incidence angle. The base moment in the y-direction is found extreme of 1.95 for model-A at 45° and 135° wind angle while for model-C the maximum C_{My} is 0.36 at 90° and for model having round corner in each limb of Y-shape is having the maximum C_{My} of 0.34 at the 90°- wind incidence angle. Base moment along x and y direction are C_{M_x} & C_{M_y} where M_x and M_y is the base moment obtained through the numerical simulation, U_h is the reference wind speed at height h, A_p is the projected area and H is the height of the building model.

4. Conclusion

This research study is performed using ANSYS CFX on various shape building models and presents the comparison between regular and irregular shape building models having different corner configurations. The results obtained through numerical techniques is validated with the experimental results and different international standards. The significant outcomes from the present study are noted as follows.

- The validation study shows the very prominent results for model-1, model-2 and model-3, also the results obtained for C_{Pmean} are found significantly in the closer range with experimental as well as with different international standards.
- Pressure distribution along the peripheral distance for building model having equal cross-sectional area are discussed and presented in the graphical form for

model-A, model-B, model-C and model-D at the interval of 15° for the wind incidence angle varies between 0° to 180°.

- While comparing the models- C & D, maximum pressure along the peripheral distance found in model-D and in the case of model-A & B, the maximum positive pressure is observed for model-B, out of all four models, the model- D is having lesser pressure than the model- B.
- Out of all models, the model having round in corner Y-shape has the minimum overall base moment which is 24 % less than the model-A rectangular chamfer. Model-A & B which is having equal number of faces, the lowest external pressure coefficient is observed for model-B in the case of 15° wind incidence angle. On comparing model-C & D, model-D is more aerodynamic with respect to model-C.
- The present study is comparing the result of equal cross sectional area buildings. The dimensions of the modifications are kept same for all model and it is found that the minimum drag force is obtained for model-D which is having round corner in each limb of Y-shape.

Acknowledgement

Authors would like to express their sincere gratitude to Delhi Technological University, Delhi, India for providing funding to conduct the research work. Thanks are due to the DTU, Delhi for providing resources and research fellowship for the first author under Institutional Fellowship.

Data availability statement All data, models and code generated or used during the study appeared in the submitted article. Data are available in the form of tables and graphs.

References

[1] ASCE: 7-16 2017 *Minimum Design Loads and Associated Criteria for Buildings and Other Structures.* Structural Engineering Institute of the American Society of Civil Engineering Reston

[2] AS/NZS:1170.2 2011: Structural Design Actions - Part 2: Wind actions Standards Australia/Standards New Zealand, Sydney

[3] GB 50009-2001: National Standard of The People's Republic of China

[4] NSCP C101-15: 2015 National Structural Code of the Philippines

[5] IS: 875- Part-3 2015 Code of Practice for Design Loads (other than earthquake loads) for buildings and structures-wind loads. India

[6] EN 1991-1-4 (2005)/AC: 2010 (E) European Standard Eurocode 1: Actions on structures - Part 1-4: General actions Wind actions European Committee for Standardization (CEN) Europe

[7] MNBC MYANMAR NATIONAL BUILDING CODE Part 3 and Part 4 2020 International relation and legal Section, Department of Building, Ministry of Construction

[8] ASCE: 49-12 2012 Wind Tunnel Testing for Buildings and Other Structures.Structural Engineering Institute of the American Society of Civil Engineering, Reston. *American Society of Civil Engineers* 1801 Alexander Bell Drive Reston Virginia

[9] ASCE Manuals and Reports on Engineering practice No. 67: 1999 *Wind Tunnel Studies of Buildings and Structures*

[10] Versteeg H K and Malalasekera W 1995 An introduction to Computational Fluid Dynamics the Finite Volume Method. Springer, England

[11] Ferziger J H and Peric M 2002 *Computational Methods for Fluid Dynamics,* Germany

[12] John D Anderson J 2010 *Computational Fluid Dynamic*, second edition. Singapore

[13] Nagar S K, Raj R and Dev N 2020 Experimental study of wind induced pressures on tall buildings of different shapes. *Wind Struct.* 31: 441–453. https://doi.org/10.12989/was.2020.31.5.441

[14] Kwok K C S 1988 Effect of building shape on wind-induced response of tall building. *J. Wind Eng. Ind. Aerodyn.* 28: 381–390. https://doi.org/10.1016/0167-6105(88)90134-1

[15] Blessmann J and Riera J D 1985 Wind excitation of neighbouring tall buildings. *J. Wind Eng. Ind. Aerodyn.* 18: 91–103. https://doi.org/10.1016/0167-6105(85)90076-5

[16] Pal S, Raj R and Bilateral Anbukumar S 2021 Interference of wind loads induced on duplicate building models of various shapes. *Latin Am. J. Solids Struct.*. https://doi.org/10.1590/1679-78256595

[17] Sharma A, Mittal H and Gairola A 2018 Mitigation of wind load on tall buildings through aerodynamic modifications. *J. Build. Eng.* 18: 180–194. https://doi.org/10.1016/j.jobe.2018.03.005

[18] Yi J and Li Q S 2018 Wind tunnel and full-scale study of wind effects on a super-tall building. *J. Fluids Struct.* 58: 236–253. https://doi.org/10.1016/j.jfluidstructs.2015.08.005

[19] Bairagi A K and Dalui S K 2018 Comparison of aerodynamic coefficients of setback tall buildings due to wind load. *Asian J. Civ. Eng.* 19: 205–221. https://doi.org/10.1007/s42107-018-0018-3

[20] Bhattacharyya B and Dalui S K 2018 Investigation of mean wind pressures on 'E' plan shaped tall building. *Wind Struct.* 26: 99–114. https://doi.org/10.12989/was.2018.26.2.099

[21] Bearman P W and Morel T 1983 Effect of free stream turbulence on the flow around bluff bodies. *Prog. Aerosp. Sci.* 20: 97–123. https://doi.org/10.1016/0376-0421(83)90002-7

[22] Raj R and Ahuja A K 2013 Wind loads on cross shape tall buildings. *J. Acad. Ind. Res.* 2: 111–113

[23] Raj R, Sharma A and Chauhan S 2018 Response of square and plus shaped buildings on varying wind loads. *Urban. Chall. Emerg. Econ.*. https://doi.org/10.1061/9780784482032.022

[24] Li Y, Li Q S and Chen F 2017 Wind tunnel study of wind-induced torques on L-shaped tall buildings. *J. Wind Eng. Ind. Aerodyn.* 167: 41–50. https://doi.org/10.1016/j.jweia.2017.04.013

[25] Blackmore P A 1997 The role of wind tunnel testing in the design of building structures. *Proc Inst. Civ. Eng. Struct. Build.* 122: 253–265. https://doi.org/10.1680/istbu.1997.29797

[26] Hui Y, Yoshida A and Tamura Y 2013 Interference effects between two rectangular-section high-rise buildings on local peak pressure coefficients. *J. Fluids Struct.* 37: 120–133. https://doi.org/10.1016/j.jfluidstructs.2012.11.007

[27] Pal S and Raj R 2021 Evaluation of wind induced interference effects on shape remodeled tall buildings. *Arab. J. Sci. Eng.* 46: 11425–11445. https://doi.org/10.1007/s13369-021-05923-x

[28] Zu G B and Lam K M 2018 Across wind excitation mechanism for interference of twin tall buildings in staggered arrangement. *J. Wind Eng. Ind. Aerodyn.* 177: 167–185. https://doi.org/10.1016/j.jweia.2018.04.019

[29] Nagar S K, Raj R and Dev N 2021 Proximity effects between two plus plan shaped high-rise buildings on mean and RMS pressure coefficients. *Sci. Iran.* https://doi.org/10.24200/sci.2021.55928.4484

[30] Gaur N, Raj R and Goyal P K 2021 Interference effect on corner configured structures with variable geometry and blockage configurations under wind loads using CFD. *Asian J. Civ. Eng.* 22: 1607–1623. https://doi.org/10.1007/s42107-021-00400-0

[31] Rajasekarababu K B, Vinayagamurthy G and Selvi Rajan S 2019 Experimental and computational investigation of outdoor wind flow around a setback building. *Build. Simul.* 12: 891–904. https://doi.org/10.1007/s12273-019-0514-8

[32] Taniguchi K and Akamine Y 2020 Wind pressure coefficient distribution of detached houses in a dense residential block. *Japan Archit. Rev.* 3: 629–645. https://doi.org/10.1002/2475-8876.12173

[33] Zheng D, Zhang A and Gu M 2012 Improvement of inflow boundary condition in large eddy simulation of flow around tall building. *Eng. Appl. Comput. Fluid Mech.* 6: 633–647. https://doi.org/10.1080/19942060.2012.11015448

[34] Haque M N, Katsuchi H, Yamada H and Nishio M 2014 Investigation of flow fields around rectangular cylinder under turbulent flow by LES. *Eng. Appl. Comput. Fluid Mech.* 8: 396–406. https://doi.org/10.1080/19942060.2014.11015524

[35] Gaur N and Raj R 2021 Aerodynamic mitigation by corner modification on square model under wind loads employing CFD and wind tunnel. *Ain Shams Eng. J.* 13: 101521. https://doi.org/10.1016/j.asej.2021.06.007

[36] Mou B, He B J, Zhao D X and Chau K W 2017 Numerical simulation of the effects of building dimensional variation on wind pressure distribution. *Eng. Appl. Comput. Fluid Mech.* 11: 293–309. https://doi.org/10.1080/19942060.2017.1281845

[37] Hu P, Li Y, Han Y, Cai S C S and Xu X 2016 Numerical simulations of the mean wind speeds and turbulence intensities over simplified gorges using the SST K-ω turbulence model. *Eng. Appl. Comput. Fluid Mech.* 10: 359–372. https://doi.org/10.1080/19942060.2016.1169947

[38] Blocken B, Stathopoulos T and Carmeliet J 2007 CFD simulation of the atmospheric boundary layer: wall function problems. *Atmos. Environ.* 41: 238–252. https://doi.org/10.1016/j.atmosenv.2006.08.019

[39] Bairagi A K and Dalui S K 2021 Estimation of Wind Load on Stepped Tall Building Using CFD Simulation. *Iran. J. Sci. Technol. Trans. Civ. Eng.* 45: 707–727. https://doi.org/10.1007/s40996-020-00535-1

[40] Kumar A and Raj R 2021 Study of pressure distribution on an irregular octagonal plan oval shape building using CFD. *Civ. Eng. J.* 7: 1787–1805. https://doi.org/10.28991/cej-2021-03091760

[41] Okajima A 1982 Strouhal number of rectangular cylinders. *J. Fluid Mech.* 123: 379–398. https://doi.org/10.1017/S0022112082003115

[42] Mallick M, Mohanta A, Kumar A and Raj V 2018 Modelling of wind pressure coefficients on C shaped building models. *Model. Simul. Eng.* 2018: 6524945. https://doi.org/10.1155/2018/6524945

[43] Stathopoulos T and Baskaran B A 1996 Computer simulation of wind environmental conditions around buildings. *Eng. Struct.* 18: 876–885. https://doi.org/10.1016/0141-0296(95)00155-7

[44] Cheng X, Huang G, Yang Q and Zhou X 2021 Influence of architectural facades on wind pressures and aerodynamic forces of tall buildings. *J. Struct. Eng.*. https://doi.org/10.1061/(asce)st.1943-541x.0002867

[45] Bhattacharjee S, Banerjee S, Majumdar S G, Dey A and Sanyal P 2021 Effects of irregularity on a butterfly plan shaped tall building under wind load. *J. Inst. Eng. (India) Ser. A* 102: 451–467. https://doi.org/10.1007/s40030-021-00511-6

[46] Tang J W, Xie Y M, Felicetti P, Tu J Y and Li J D 2010 Numerical simulations of wind drags on straight and twisted polygonal buildings. *Struct. Des. Tall Special Build.* 22: 62–73. https://doi.org/10.1002/tal.657

[47] Zheng C R and Zhang Y C 2010 Numerical investigation on the drag reduction properties of a suction controlled high-rise building. *J. Zhejiang Univ. Sci. A.* 11: 477–487. https://doi.org/10.1631/jzus.A0900593

[48] Bairagi A K and Dalui S K 2021 Wind environment around the setback building models. *Build. Simul.* 14: 1525–1541. https://doi.org/10.1007/s12273-020-0758-3

[49] Raj R, Jha S, Singh S and Choudhary S 2020 Response analysis of plus shaped tall building with different bracing systems under wind load. *Int. J. Adv. Res. Eng. Technol.* 11: 371–380. https://doi.org/10.34218/IJARET.11.3.2020.032

[50] ANSYS 2020 CFX Solver Modeling Guide Europe

[51] ANSYS 2010 Meshing User Guide Europe

[52] Abu Zidan Y, Mendis P and Gunawardena T 2021 Optimising the computational domain size in CFD simulations of tall buildings. *Heliyon* 7: e06723. https://doi.org/10.1016/j.heliyon.2021.e06723

[53] Revuz J, Hargreaves D M and Owen J S 2012 On the domain size for the steady-state CFD modelling of a tall building. *Wind Struct.* 15: 313–329. https://doi.org/10.12989/was.2012.15.4.313

[54] Raj R 2015 *Effects of cross-sectional shapes on response of tall buildings under wind loads*. Doctorate of Philosophy, Indian Institute of Technology Roorkee, Roorkee

[55] Amin J A and Ahuja A K 2013 Effects of side ratio on wind-induced pressure distribution on rectangular buildings. *J. Struct.*. https://doi.org/10.1155/2013/176739

[56] Sanyal P and Dalui S K 2018 Effects of courtyard and opening on a rectangular plan shaped tall building under wind load. *Int. J. Adv. Struct. Eng.* 10: 169–188. https://doi.org/10.1007/s40091-018-0190-4

[57] Kumar D and Dalui S K 2017 Effect of internal angles between limbs of cross plan shaped tall building under wind load. *Wind Struct.* 24: 95–118. https://doi.org/10.12989/was.2017.24.2.095

[58] ETHIOPIAN STANDARD: ES ISO 4354 2012 English Wind actions on structures

[59] Celik I B, Ghia U, Roache P J, Freitas C J, Coleman H and Raad P E 2008 Procedure for estimation and reporting of uncertainty due to discretization in CFD applications. *J. Fluids Eng. ASME* 130: 0780011–0780014. https://doi.org/10.1115/1.2960953

[60] Derakhshandeh J F and Alam M M 2018 Flow structures around rectangular cylinder in the vicinity of a wall. *Wind Struct.* 26: 293–304. https://doi.org/10.12989/was.2018.26.5.293

[61] Haller G 2005 An objective definition of a vortex. *J. Fluid Mech.* 525: 1–26. https://doi.org/10.1017/S0022112004002526

[62] Zheng X, Montazeri H and Blocken B 2021 CFD analysis of the impact of geometrical characteristics of building balconies on near-façade wind flow and surface pressure. *Build. Environ.* 200: 107904. https://doi.org/10.1016/j.buildenv.2021.107904